Impact Location Dependence of Behind Armor Blunt Trauma Injury Assessed using a Human Body Finite Element Model

Michael C. Bustamante[1], Duane S. Cronin[2]

[1]Department of MME, University of Waterloo, 200 University Ave. West, Waterloo, N2L 3G1 Canada, mcbustam@uwaterloo.ca

[1]Department of MME, University of Waterloo, 200 University Ave. West, Waterloo, N2L 3G1 Canada, dscronin@uwaterloo.ca

Submitted to: Journal of Biomechanical Engineering

Corresponding Author: Dr. Duane S. Cronin
Department of Mechanical and Mechatronics Engineering
University of Waterloo
200 University Ave. West
Waterloo, Ontario, Canada, N2L 3G1
dscronin@uwaterloo.ca
(519) 888-4567 x32682

Word Count: 5056 (Introduction to Conclusions)

1 Abstract

Behind Armor Blunt Trauma (BABT), resulting from dynamic deformation of protective ballistic armor into the thorax, is currently assessed assuming a constant threshold of maximum backface deformation (44 mm). Although assessed for multiple impacts on the same armor, testing is focused on armor performance (shot-to-edge and shot-to-shot) without consideration of the underlying location on the thorax. Previous studies identified the importance of impacts over organs of animal surrogates wearing soft armor. However, the effect of impact location was not quantified outside the threshold of 44 mm. In the present study, a validated biofidelic advanced human thorax model (50^{th} percentile male) was utilized to assess the BABT outcome from varying impact location. The thorax model was dynamically loaded using a method developed for re-creating BABT impacts, and BABT events within the range of real-world impact severities and locations were simulated. It was found that thorax injury depended on impact location for the same BFDs. Generally, impacts over high compliance locations (anterolateral rib cage) yielded increased thoracic compression and loading on the lungs leading to pulmonary lung contusion. Impacts at low compliance locations (top of sternum) yielded hard tissue fractures. Injuries to the sternum, ribs, and lungs were predicted at BFDs lower than 44 mm for low compliance locations. Location-based injury risk curves demonstrated greater accuracy in injury prediction. This study quantifies the importance of impact location on BABT injury severity and demonstrates the need for consideration of location in future armor design and assessment.

Keywords: Behind Armor Blunt Trauma, Impact Location Dependence, Injury Risk Curves, Hard Tissue Fracture, Lung Contusion, Thorax Finite Element Model, Impact Re-creation

2 Introduction and Background

2.1 Introduction

The goal of bullet-resistant vests or soft armor is to protect the wearer from small-caliber projectiles while maintaining their mobility [1]. Layers of flexible armor fabric (e.g., Aramid) protect by absorbing the energy of the projectile through deformation, preventing perforation of the vest while arresting the projectile. The greatest extent of the deformation to the wearer's thorax, or in the case of laboratory testing, the backing material (e.g., clay and gelatin), is known as the Backface Deformation (BFD), sometimes called the backface signature. Contemporary soft armor is

assessed at specific impact locations with the vest evaluated on a clay backing [2], without the consideration of the underlying tissues at the impact locations. Although soft armor can be successful in arresting a projectile without perforation, vest deformation into the body can result in high-rate compression of the underlying tissues leading to contusion and laceration of thoracic soft tissues, or fracture of hard tissues (ribs or sternum), known as behind armor blunt trauma (BABT) [3,4].

Early BABT studies investigated the performance of soft armor using animal surrogates, impacted over vulnerable organs, for correlation with human BABT injuries [5]. These studies proposed test methods to measure soft armor BFDs for BABT events using clay or ballistic gelatin as the backing material. The measured BFDs could then be correlated with injuries from the animal surrogates that underwent comparable BABT events, and then ultimately scaled to humans [1]. A result of those studies was proposing BFD measured in clay as a single metric for evaluating armor performance.

Other studies suggested the use of alternative metrics in correlating injuries such as energy density [6], viscous criterion, and blunt criterion [7,8], all of which required additional measurements of the BABT event (e.g., projectile velocity) and the target involved (e.g., mass). Current methods of testing soft body armor use BFD measured using a clay backing material [2].

2.2 Soft Armor Assessment

A soft armor BFD of 44 mm measured on a clay backing is a pass/fail criterion for soft armor protection assessment [2]. The origin of the 44 mm comes from research in the 1970s that aimed to correlate human BABT with experimental tests of 0.38-special and 0.22 caliber projectiles on goats donned with 7-ply Kevlar soft armor [5,9]. Clare [10] reported a correlation model between the goat injuries and BFD measurements in Roma Plastilina no.1 clay. This correlation was necessary due to the inability to measure BFD directly on the animal surrogates. Prather [1] reported the impacts on goats that corresponded to impacts of 44 mm BFD in clay demonstrated a lack of severe injury in the goat, only yielding a 6% probability of lethality. Given the size of a human man (~70 kg) is greater than that of the goats assessed (40-50 kg), the study concluded that 44 mm BFD could be used as a conservative threshold for limiting BABT in humans.

Based on publicly available literature, there is little evidence of lethality as a result of BABT when the impacts are within the design considerations of the soft armor [11]. However, an understudied aspect of BABT is the difference in response from impacts at varying locations on the human thorax. Goldfarb [5] impacted goats at vulnerable areas of the body: the heart, spine, lung, liver, gut, and spleen, but many assumptions were made when using the data to calculate the lethality risk of a human. A later study by Carroll [3] qualitatively compared the reported goat injury results with nonlethal real-world BABT injuries from policemen. However, the reported injuries were not correlated with BABT metrics. More recently, Jennings [12] conducted soft armor impacts on a pig thorax, targeting the spine, and found that spinal BABT could lead to serious injury due to vertebral fractures and proximity to the spinal cord as compared to anterior BABT.

2.3 BABT Survivor Cases and Re-Creation Testing

The compilation of epidemiological databases containing BABT events and injuries provides critical data to understand BABT injuries in humans. Such databases provide an important link to correlate laboratory parametric studies from non-human surrogates to live humans, as well as provide a more relevant comparison to historical animal models. An example of such a database is the BABT Injury Database (BABT-ID) which reported forty-seven real-world soft armor BABT impact cases from law enforcement officers [13,14]. The BABT-ID reported survivors of BABT events and their injuries with the corresponding event parameters, such as type of armor, impact location, medical records, stand-off distance, and type of projectile. An injury scale was developed specifically for the BABT-ID that focused on clinically significant injuries. The levels included: minor (bruising and minor wound care), moderate (bruising, lung contusion, and open wound care), and severe (internal injuries requiring medical intervention and advanced wound care). Moderate and severe injuries were considered clinically significant. Scenarios in the BABT-ID were re-created in the laboratory using the known BABT event parameters, such as armor type, standoffs, and projectiles on clay backing. The measured BFDs from the re-creations were correlated to the clinically significant injuries reported in the medical records. Interestingly, it was reported that a BFD of 43.6 mm corresponded to a 50% risk of a clinically significant injury, in line with the soft armor threshold of 44 mm used in test standards.

2.4 Finite Element Models to Assess BABT

Recent studies have used biofidelic advanced human body finite element models (FE) to address previous limitations of using animal models for predicting the potential for injury. Early verification and validation studies in the literature

report using contemporary human body models by exercising the models with similar impacts expected in BABT, then assessed for injury by way of soft and hard tissue damage. In most cases, the human body model was developed for a different purpose such as automotive crashes and required validation of biofidelity for higher rate BABT deformation.

Roberts [15–17] and Merkle [18] assessed the Human Torso Finite Element Model (HTFEM) and in parallel a physical surrogate known as the Human Surrogate Torso Model (HSTM). Both models were impacted at three impact locations with a qualitative examination of pressure and energy in vulnerable organs and response to vests with increasing levels of threat protection. Raftenberg [19] investigated the efficacy of the Wayne State Thorax Model (WSTM) in re-creating BABT events and modeling armor vest fabric. Similarly, Shen [20] modeled a projectile and soft armor BABT event on a human thorax model. In general, these human models were in their development stage and did not include specific injury risk outcomes or model validation, and therefore reported comparative or qualitative results. Cronin [8,21] performed BABT impacts on early versions of the BABT-WALT (Waterloo Thorax) model, identifying sensitivity to impact velocity and dynamic deformation of the armor. The BABT-WALT model is an advanced human body thorax model to assess BABT and includes a detailed thoracic cage, heart, lungs, and muscle tissue (Fig. 1). The model was enhanced for high deformation loading and validated with pendulum impacts and less lethal kinetic weapon impact experiments on post-mortem human subjects (PMHS).

A more recent study by Cronin [4] further developed the BABT-WALT thorax model (Version v7-2) to predict pulmonary lung contusion (PLC), sternum, and rib fractures, and then validated the model using ten re-created real-world cases of BABT events from the BABT-ID. Sternum and rib fractures were predicted using strain-based deterministic failure criterion, and PLC using maximum transient hydrostatic stress (pressure) in the lung elements. The transient pressure threshold was 45.5 kPa, determined from a 6.7 m/s pendulum impact on the thorax leading to AIS 3 level injury (Viano et al. 1989), and corresponding to acute respiratory distress syndrome (20% contusion by volume) (Miller et al. 2001, Becher et al. 2012).

A novel method of applying BABT impacts to the thorax model was developed using an evolving deformation boundary condition directly measured from soft armor impacts. This novel method, described as the BABT impact boundary condition (BIBC), simulated impacts of the ten BABT-ID cases using BFD histories measured from re-created impacts on 10% ballistic gelatin blocks with case-specific projectile and armor. An injury scale was developed

based on the literature, using the predicted hard tissue and PLC injuries. The levels included: minor (no fracture and total volume PLC was less than 10%), moderate (one fracture event or total volume PLC was between 10% and 20%), and severe (two or more fracture events or total PLC greater than 20%). Re-creation of the ten real-world cases with the BABT-WALT model integrated with the BIBC resulted in predicted injuries comparable to those reported in the BABT-ID.

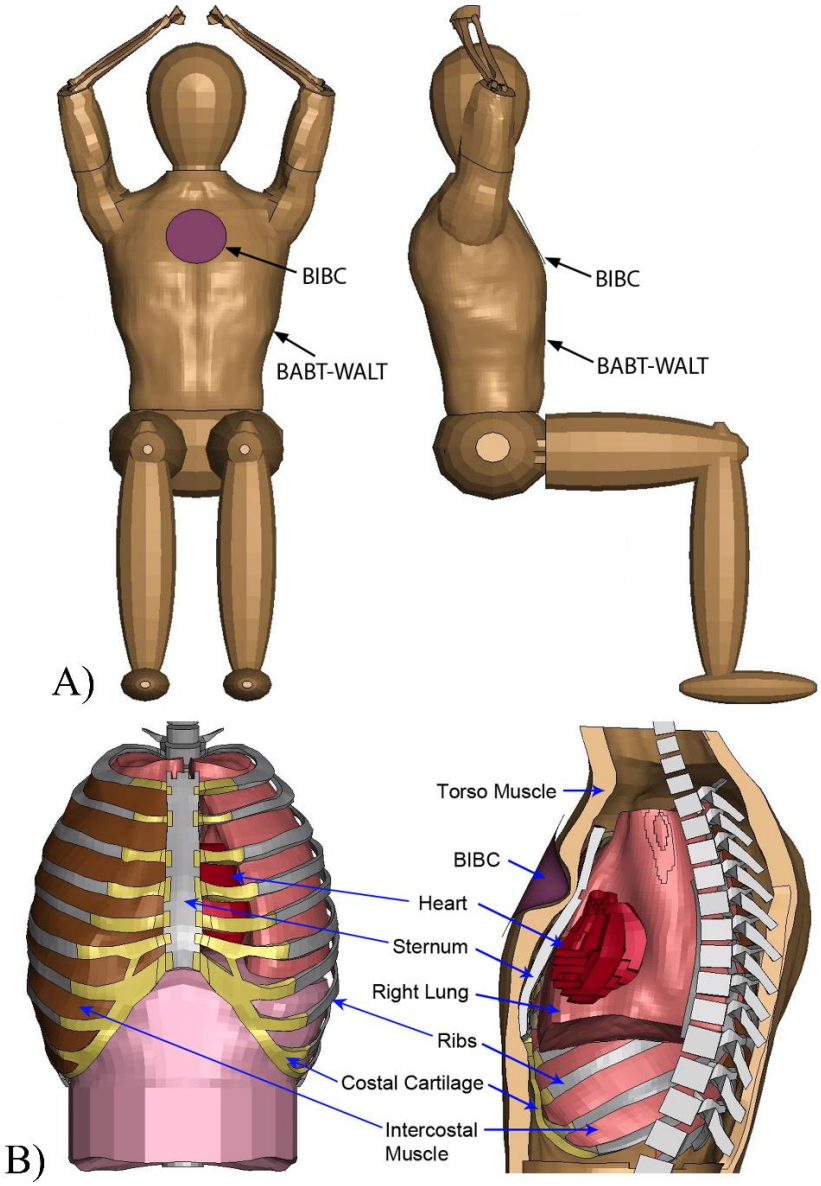


Fig. 1: A) BABT-WALT FE model with detailed thorax including thoracic cage; front and side view with BIBC. B) Thoracic cage with left-side intercostal muscle removed to show left lung and heart, along with an example of BIBC loading as a cross-section.

In the present study, a previously validated method of simulating BABT impacts (BIBC) on a detailed thorax model (BABT-WALT) [4] was used to investigate varying impact locations and corresponding injury severity. Eight impact locations, corresponding to the range reported in the BABT-ID database were identified and assessed for three impact severities (24 total cases). Response metrics including deformation, peak-force, total impulse, and work, were calculated and compared using the resulting tissue-level injuries (rib fracture, sternum fracture, and PLC). Lastly, injury risk curves (IRCs) were fit to the different response metrics for the whole thorax and for each of the eight impact locations to assess locational dependence.

3 Methods

3.1 Numerical Methodology using the BABT-WALT and BIBC

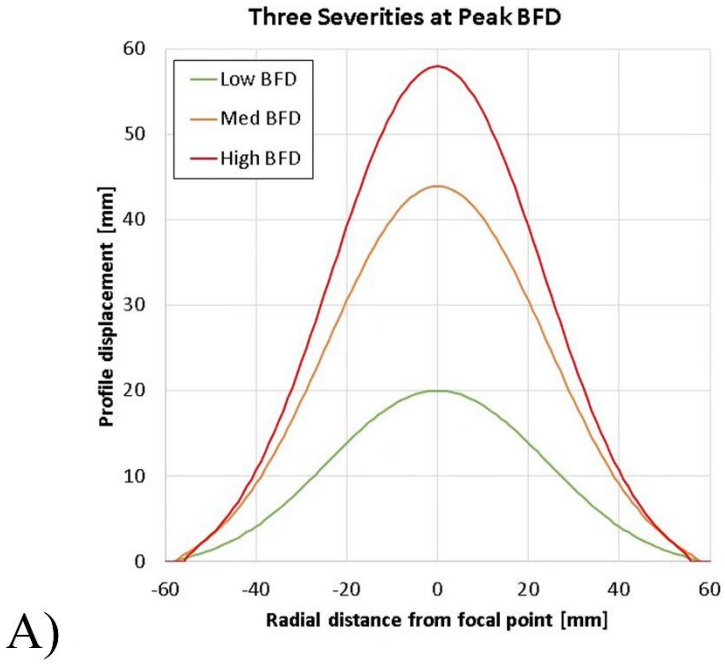
This study used the BABT-WALT model with the BIBC loading method for simulating BABT (Fig. 1). Three different impact severities were simulated at eight impact locations on the thorax. The BIBC loading condition was modeled as a circular plate using radially diverging elements with a total diameter of 120 mm, with prescribed displacement to mimic the BABT event. Smaller elements were concentrated at the center of the plate since the largest deformation gradients occurred at the focal point of the BABT impact. Injurious were considered as the occurrence of one or more hard or soft tissue injuries. Hard or soft tissue injuries were identified using the method reported by Cronin [4] and are as follows. A hard tissue injury was considered as the presence of one or more instance of rib or sternum fracture. A rib or sternum fracture event was predicted to initiate when an element in the tissue reached a critical plastic strain and was eroded. A soft tissue injury was considered with PLC was greater than 10% [4]. PLC was calculated as a volume percentage lung element exceeding a threshold transient hydrostatic pressure of 45.5 kPa.

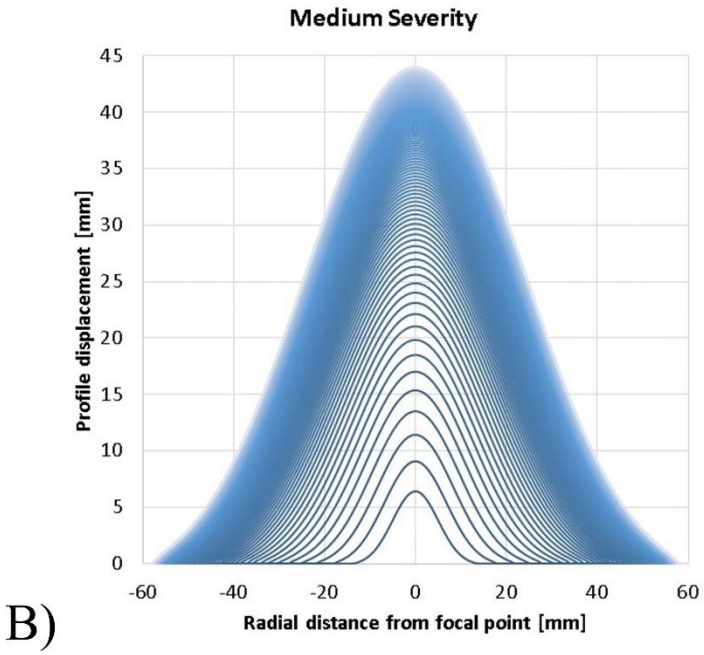
An advantage of using FE models to simulate BABT events was the ability to measure deformation at different depths within the thorax. In this study, two deformation measurements were taken. The first was the BFD, measured as a peak displacement of the thoracic outer tissue at the point of impact. The second was the submuscular BFD (sBFD),

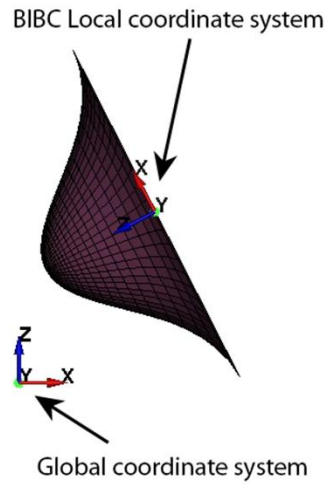
measured as the peak displacement of the thoracic cage, so that this measure excluded through-thickness compression of the muscle, adipose tissue, and skin. Additionally, the peak-force, total impulse, and work of the impact were calculated from the contact force between the outer surface of the thorax and the BIBC loading condition. Total impulse was taken as the peak value of the contact force-time integral, and work was taken as the peak value of the cumulative sum of contact force times the plate displacement until loss of contact with the thorax.

3.2 Parameterized Loading Conditions for BIBC Impact Study

The three impact severities investigated were: low, medium, and high, corresponding to 20 mm [13], 44 mm [2], and 58 mm [1,22–24] peak displacements, respectively (Fig. 2A). The low-severity of 20 mm was considered because it was equivalent to the BFD that transitioned between a minor and a moderate injury reported in the BABT-ID. A medium severity of 44 mm corresponded to the standard BFD pass/fail criterion for soft armor on clay backing (Fig. 2B). Lastly, the high severity of 58 mm was considered because it was within the upper range of BFD values reported in the literature that studied soft armor with varying backings. The BABT responses were mapped onto the surface of the BIBC plate mesh by prescribing displacement histories to the nodes of the mesh within the local coordinate system (Fig. 2C). Due to the complex topography of the thorax, the BIBC plate was positioned to be parallel to the thorax surface and to minimize standoff of the plate from the thorax muscle. It should be noted that standoff between the armor and thorax may occur in physical armor fitting [25,26]. However, was not intentionally re-created for this study.







176

177 ***Fig. 2. A) Profile of the three BABT impact severities at BFD or peak displacement, B) Profiles of the medium***

178 ***severity at increasing time (0.03 ms increments) until peak displacement, C) Local coordinate system of the BIBC***

179 ***plate relative to the global coordinate system.***

180

3.3 BABT Impact Locations on the Thorax Model

Eight impact locations were investigated on the thorax model (Fig. 3). All impact case models were solved using a commercial FE code (LS-DYNA, version 7.1.2, LST, Livermore, CA) with a simulation duration of 100 ms, encompassing the entire loading and unloading of the BABT event. The eight locations were selected to cover the range of impacts observed in real-world cases from the BABT-ID and included a variety of soft and hard tissues during the impact. Only one side of the thorax was considered due to the symmetry of the thorax, although there is asymmetry caused by the heart and lungs, and such effects will be investigated in a future study. The locations were identified using a grid-like naming convention with A, B, and C indicating the medial direction (columns) and 1, 2, and 3 indicating the inferior direction (rows).

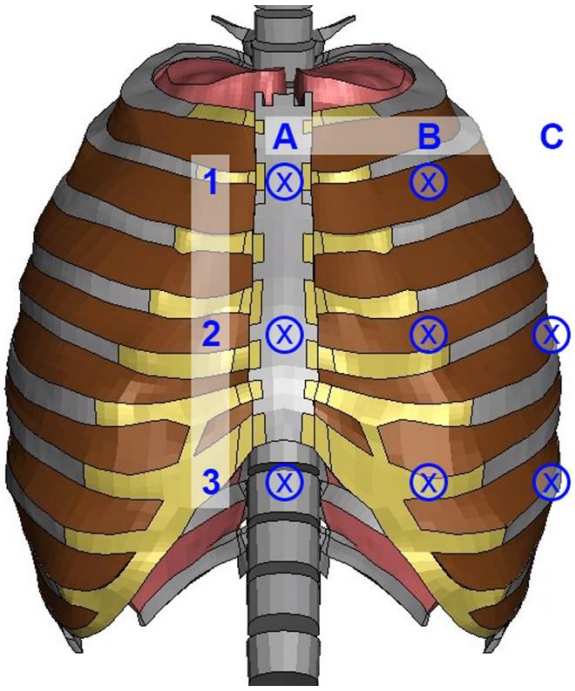


Fig. 3. Impact locations on the anterior and lateral thoracic cage with column (A, B, C) and row (1, 2, 3) identifiers.

3.4 Injury Risk Curves for Response Metrics

IRCs were calculated from the simulation data [27]. The predictive metrics considered for injury were the five response metrics: BFD, sBFD, peak force, total impulse, and work. All non-injurious cases were right-censored, and

all injurious cases were considered interval-censored, resulting in a binary outcome of 0 (non-injurious) and 1 (injurious), respectively. Interval censoring was performed because the exact value of a metric to initiate injury was unknown. However, for a given injury at a specific location, the lower bound and upper bound of impact severity was known. This method was used because of the repeatability of the model and metric values below non-injurious cases should continue to yield non-injurious responses. In addition, receiver-operating characteristic (ROC) analysis was used to determine the accuracy of the IRCs calculated [28]. Specifically, the area under the curve (AUC) of the ROC was calculated, where an AUC of 0.5 corresponds to random chance and 1.0 corresponds to ideal accuracy.

4 Results and Discussion

4.1 Location-Based Thorax Response and Injury Assessment

The twenty-four BABT simulations (Table 1) all ran to completion without any errors. The measured BFDs for each impact severity, measured as a peak displacement of the thoracic outer muscle at the point of impact, were within a range of approximately 10 mm for each impact condition (low: 10.1 – 19.6 mm; medium: 33.7 – 43.7 mm; high: 48.1 – 58.7 mm). The resulting BFDs were equal to or slightly smaller than their BIBC inputs, owing to the small but varying geometric offset between the shape of the outer thorax tissue and BIBC plate, and continued deformation from inertia of the impacted zone. All low severity cases were non-injurious, whereas the medium and high impact cases demonstrated a transition between non-injurious and injurious. All cases were plotted with respect to their location and binary coded injuries (Fig. 4). The results demonstrated an increased occurrence of injury with increasing impact severity. Furthermore, certain locations (e.g., B2 and A3) consistently showed no injuries, indicating that the location of impact may have an effect on the resulting injury outcome. Notably, cases A1-medium, C3-medium, and C2-medium yielded sternum fracture, rib fracture, and PLC injuries, respectively, with BFDs below 44 mm. Of the twenty-four cases, three cases had sternum fractures, six had rib fractures, and five had PLC. In total, nine cases resulted in injuries. Locations A2 and C2 were both associated with PLC volume greater than 20% and a sternum and rib fracture, respectively. Locations A1 and C3 were associated with multiple rib fractures, with A1 also yielding a sternum fracture.

Variation in model injury predictions as a function of location were attributed to the stiffness and geometries of the underlying tissues that were impacted. For example, impacts on the sternum (A1 and A2) demonstrated hard tissue fractures and high kinetic-based metric values (peak-force, total impulse, and work) owing to the thin layer of muscle and high stiffness hard tissue.

It was also observed that A1 yielded lesser PLC than A2, attributed to the thoracic cage geometry, which had greater resistance to thoracic cage compression. At A1, the impact moment arm on the hard tissues that resisted compression was shorter compared to location A2. Consequently, A1 experienced a direct impact on the hard tissue, which led to hard tissue fracture, while A2 dispersed the energy by compressing surrounding tissues, such as the lungs, leading to a higher PLC.

A similar effect of thoracic cage geometry can be seen when comparing locations C2 and C3 versus B2 and B3. At C2 and C3, the impact moment arms on the ribs were shorter than at B2 and B3. The greater resistance to thoracic cage compression of C2 and C3 resulted in increased hard tissue fractures. Some variability was noted at the ribs area since the point of impact could occur over or between ribs. For example, C2 and C3 locations had similar underlying hard tissues, but the impact point at C2 was between the 5^{th} and 6^{th} rib, while the impact point at C3 was over the 8^{th} rib. The direct impact of the 8^{th} rib yielded a higher localized strain in the rib and resulted in greater hard tissue injuries at C3 compared to C2. Given the complexity and local variation in compliance of the whole thorax, it was expected that injury outcome would be affected by location. In the simulated cases, these differences in outcomes were observed as a result of varying shapes and materials of the thorax constituent parts and their interaction with each other to resist thoracic compression.

Table 1. Summary of metrics and resulting injuries measured from the simulated BABT cases.

Location ID	BIBC Maximum Displacement [mm]	BFD [mm]	Submuscular BFD [mm]	Peak-Force [kN]	Total Impulse [kN-ms]	Work [kN-mm]	Total PLC [%]	Sternum Fracture	Ribs Fractured	Injury (Binary Coded)
A1	20	13.5	8.79	3.4	2.0	21.3	0.01	0	0	0
A1	44	37.6	29.4	12.8	6.5	185.5	3.63	1	0	1
A1	58	51.8	42.4	40.3	9.2	395.6	12.79	1	2	1
A2	20	10.1	7.67	2.9	1.5	12.3	0.00	0	0	0

A2	44	33.7	29.6	24.8	9.5	229.2	8.88	0	0	0
A2	58	48.1	49.6	62.2	10.9	480.7	24.88	1	0	1
A3	20	14.6	11.8	4.3	1.3	19.2	0.00	0	0	0
A3	44	38.4	33.9	14.1	5.5	142.7	0.99	0	0	0
A3	58	52.8	48.7	15.7	8.4	285.0	2.84	0	0	0
B1	20	15.7	10.3	3.7	1.4	21.8	0.32	0	0	0
B1	44	40	30.7	12.0	4.7	137.7	5.80	0	0	0
B1	58	54	47.1	19.8	6.2	251.5	18.34	0	1	1
B2	20	19.6	14.8	4.9	1.4	32.0	0.25	0	0	0
B2	44	43.7	35.1	27.4	4.3	138.2	3.44	0	0	0
B2	58	58	46	28.5	6.5	235.7	8.11	0	0	0
B3	20	19.2	14.4	3.9	1.4	21.7	0.04	0	0	0
B3	44	43.5	35.5	12.6	4.7	123.0	1.05	0	0	0
B3	58	57.6	48.2	23.4	6.6	230.4	2.13	0	1	1
C2	20	15.4	10.7	4.1	1.5	20.5	0.41	0	0	0
C2	44	39.6	28.7	11.8	5.3	122.7	11.67	0	0	1
C2	58	53.7	44.5	19.2	6.6	217.3	26.34	0	1	1
C3	20	19.1	13.6	4.2	2.1	28.0	0.32	0	0	0
C3	44	43.7	35.7	13.7	5.1	162.4	3.09	0	1	1
C3	58	58.7	50.1	24.3	6.7	279.5	6.14	0	2	1

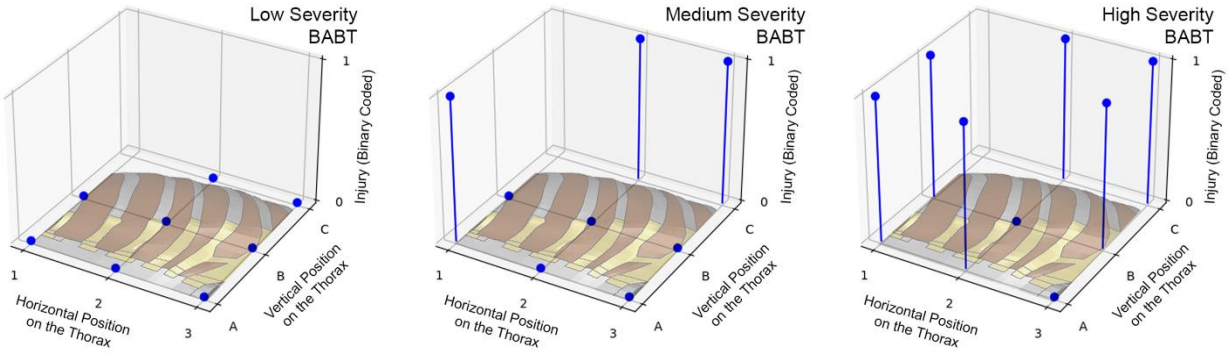


Fig. 4. Impact cases plotted for 8 locations on the thorax for three loading severities. Vertical axis is binary coded injuries, where 1 was injurious and 0 was non-injurious.

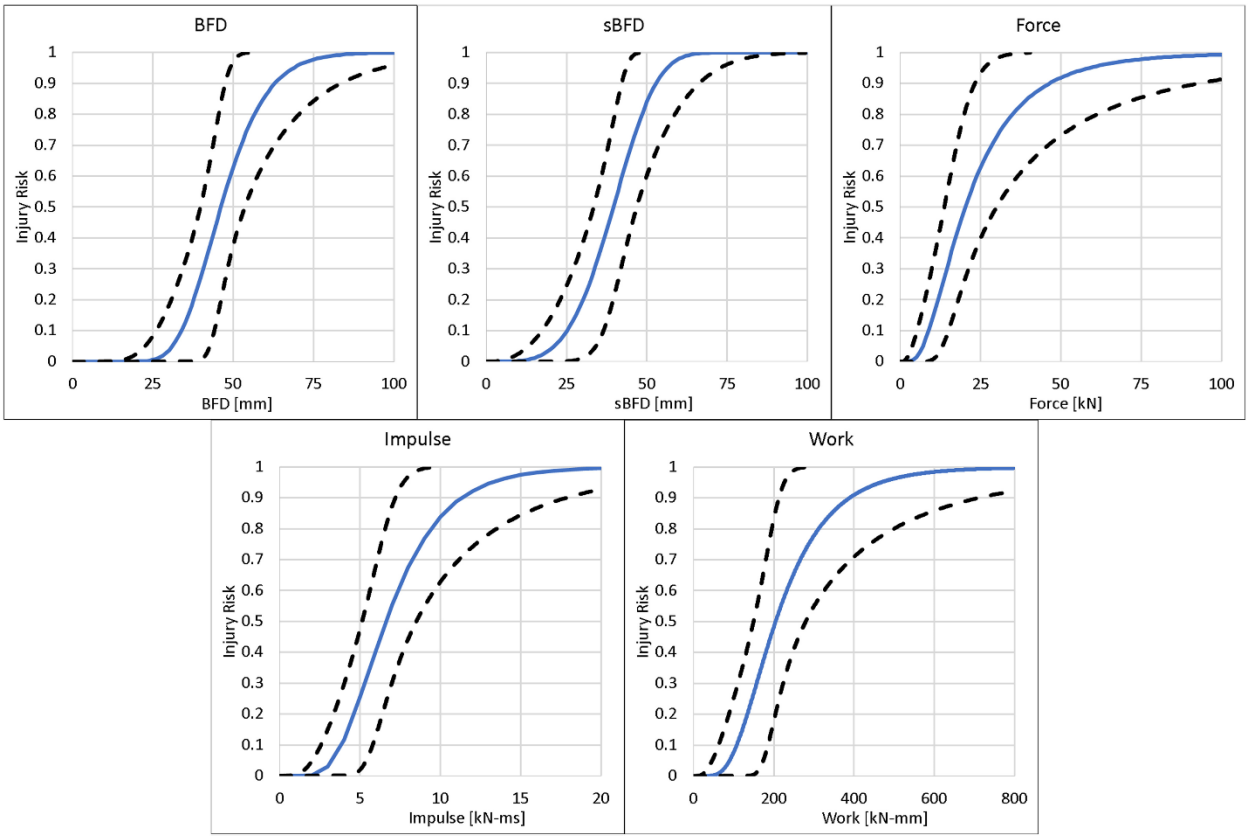
4.2 Whole Thorax Injury Risk Curves for Five Response Metrics

Whole thorax IRCs (W-IRC) along with their 95% confidence intervals (CI) were calculated for the five response metrics (Fig. 5). BFD yielded 50% injury risk at 46.2 mm with a standard error (SE) of ±3.5 mm, comparable to the

44 mm standard, and sBFD yielded 50% injury risk at 39.6 mm ±3.4 mm. Peak-force yielded a 50% injury risk at 20.2 kN with a SE of ±4.0 kN, total impulse at 6.6 kN-ms ±0.9 kN-ms, and work at 204.5 kN-mm ±32.6 kN-mm. As expected, the 50% injury threshold for sBFD (39.6 mm) was lesser than the threshold for BFD (46.2 mm), due to only considering the deformation of the thoracic cage (without the muscle). This result suggests that the thickness of the muscle and adipose tissue can play a role in the magnitude of a deformation-based injury threshold. Rafaels [7] reported an increased correlation to injury using the Blunt Criterion, which includes the chest wall thickness, relative to using BFD or volume in clay. Overall, the kinetic-based metrics yielded greater SEs and lesser quality indexes (QIs) compared to the deformation-based metrics (BFD and sBFD) (Table 2). Peak-force yielded the greatest SE of 20% as a percentage of its 50% injury risk, suggesting that force may have greater sensitivity to the impact location.

Compared to the IRC reported by Bir [13], the W-IRC for BFD in this study had a steeper slope and a narrower CI at the 50% injury risk threshold. These differences were attributed to the number of cases and type of data used by Bir. The current study used twenty-four FE cases with consistent boundary conditions, whereas Bir reported forty-seven real-life cases, which included anthropomorphic differences between the subjects and boundary condition differences. Another reason may be due to the censoring method of the real-life cases. Bir used a lower bound value of 0 for the intervals of the injurious cases because they were indeterminate, unlike the intervals in the current study using a consistent FE model.

Although the W-IRCs of the three kinetic-based metrics had greater SEs than the two deformation-based metrics, all five metrics yielded comparable accuracies (“good” discrimination) except for peak-force (“fair” discrimination) [28]. The BFD and sBFD yielded ROC AUCs of 0.848 and 0.837, respectively. Peak-force, total impulse, and work yielded ROC AUCs of 0.785, 0.852, and 0.852, respectively. For comparison, the study by Bir [13] that used forty-seven real-world cases reported an AUC of 0.70 (“fair”). The higher AUCs in this study reinforced the common outcome that real-world data contain greater variability from the different individuals, whereas the variability in this study were mainly from boundary conditions and location effects. Although sBFD may be difficult to directly measure in experimental tests, this metric was investigated to minimize the effect of outer soft tissue thickness on variability when calculating injury risk.



276

277 ***Fig. 5. W-IRCs calculated for (A) BFD, (B) submuscular BFD (sBFD), (C) peak force, (D) total impulse, and (E)***

278 ***work metrics with 95% confidence intervals shown.***

279

280 ***Table 2. Summary of W- IRCs and L-IRCs characteristics for the 5 metrics considered. Quality Index and ROC***

281 ***AUC showing Excellent (E), Good (G), Fair (F), Marginal (M), and Unacceptable (U) qualities and***

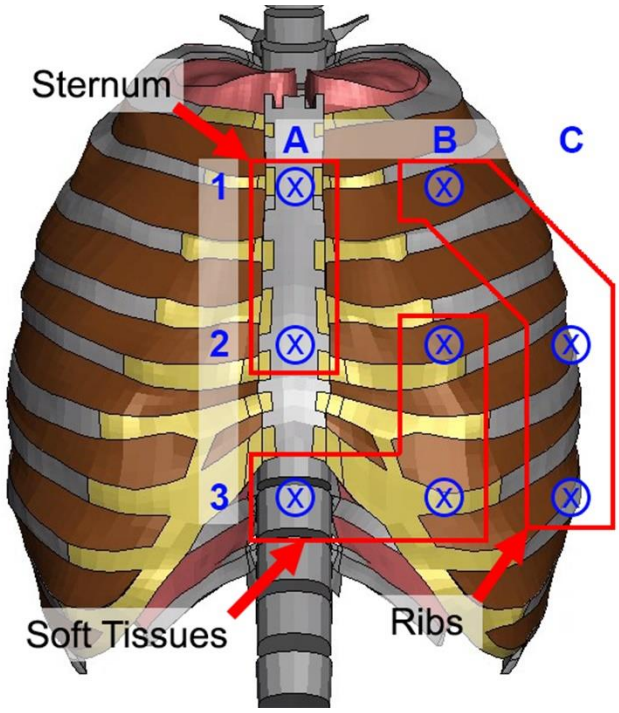
282 ***discriminations, respectively.***

	Sternum				Ribs				Soft Tissues				Whole Thorax			
Metrics	**50% ±SE**	**SE as percentage of 50%**	**QI (5%, 25%, 50%)**	**ROC AUC**	**50% ±SE**	**SE as percentage of 50%**	**QI (5%, 25%, 50%)**	**ROC AUC**	**50% ±SE**	**SE as percentage of 50%**	**QI (5%, 25%, 50%)**	**ROC AUC**	**50% ±SE**	**SE as percentage of 50%**	**QI (5%, 25%, 50%)**	**ROC AUC**
BFD	37.1	NA	NA	1.0 (E)	40.7 ±1.5	4%	0.47 (G), 0.20 (G), 0.14 (G)	0.95 (E)	57.9 ±2.5	4%	0.45 (G), 0.21 (G), 0.17 (G)	0.875 (G)	46.2 ±3.5	8%	0.82 (F), 0.41 (G), 0.29 (G)	0.848 (G)

sBFD	31.7 ±4.6	14%	1.96 (U), 0.65 (F), 0.57 (F)	0.889 (G)	31.4 ±3.1	10%	1.79 (U), 0.68 (F), 0.39 (G)	0.95 (E)	48.7 ±2.0	4%	0.39 (G), 0.16 (G), 0.16 (G)	0.875 (G)	39.6 ±3.4	9%	0.99 (F), 0.49 (G), 0.34 (G)	0.837 (G)
Force	24.9 ±9.2	37%	6.08 (U), 2.31 (U), 1.58 (U)	0.889 (G)	12.3 ±0.7	6%	0.76 (F), 0.33 (G), 0.23 (G)	0.95 (E)	33.5 ±14.7	44%	1.72 (U), 1.25 (M), 1.93 (U)	0.75 (F)	20.2 ±4.0	20%	1.35 (M), 0.83 (F), 0.80 (F)	0.785 (F)
Impulse	8.3 ±1.7	20%	3.32 (U), 1.35 (M), 0.81 (F)	0.778 (F)	5.0	NA	NA	1.0 (E)	8.6 ±2.6	30%	1.07 (M), 0.85 (F), 1.24 (M)	0.875 (G)	6.6 ±0.9	13%	1.02 (M), 0.6 (F), 0.51 (F)	0.852 (G)
Work	246.6 ±67.2	27%	4.55 (U), 1.76 (U), 1.12 (M)	0.889 (G)	139.4 ±22.5	16%	3.46 (U), 1.21 (M), 0.64 (F)	0.95 (E)	307.8 ±119.6	39%	1.61 (U), 1.12 (M), 1.68 (U)	0.75 (F)	204.5 ±32.6	16%	1.42 (M), 0.78 (F), 0.64 (F)	0.852 (G)

4.3 Injury Risk Curves for Locations with Similar Underlying Tissues at Impact Location

Additional IRCs were calculated for three locations on the thorax that had similar underlying tissues (Locational IRCs, or L-IRCs) (Table 2): sternum (A1 and A2), ribs (B1, C2, and C3), and soft tissues without supporting hard tissues (A3, B2, and B3) (Fig. 6). Locations B2 and B3 were considered to be within the soft tissues area because they also included costal cartilage, which is less stiff relative to the sternum and ribs. The five metrics were assessed at each of the three locations (total of fifteen L-IRCs). The SE and QI could not be calculated for the sternum location BFD and the rib location total impulse due to their data points resulting in stepwise area L-IRCs (Table 2).



292

293 ***Fig. 6. Impact locations grouped into areas with similar underlying tissues.***

294

295 Relative to their W-IRCs, the five metrics generally yielded greater SEs at the sternum area and lesser SEs at the ribs
296 area (Table 2). For the soft tissue location, the results were mixed with the deformation-based metrics yielding lesser
297 SEs and the kinetic-based metrics yielding greater SEs compared to their W-IRCs. Four L-IRCs had improved SEs
298 and QIs (BFD at ribs and soft tissues, sBFD at soft tissues, and force at ribs), while the remaining nine L-IRCs had
299 greater SEs and lower QIs compared to their W-IRCs. This was expected due to the reduction in samples size for each
300 L-IRC relative to their W-IRCs.

301 For additional consideration, the accuracies of the L-IRCs were also determined via ROC analysis. Analysis of the
302 ROC curves of the fifteen L-IRCs yielded twelve having greater AUC scores compared to their W-IRCs. This included
303 the two stepwise area L-IRCs, which yielded AUC scores of 1.0. The deformation-based metrics had improved AUCs
304 for all locations and the kinetic-based metrics had improved AUCs for the ribs area, but only some for the sternum
305 area (force and work) and soft tissues area (impulse). The improvement in the majority of the AUCs suggests that
306 injury risk predictions improved when considering location.

For the deformation-based metrics, their 50% injury thresholds at the sternum and ribs were lesser than their W-IRCs, suggesting that injury prediction at the sternum and ribs may be conservative when using the whole thorax criterion. A similar finding was also reported by Shen [20] from an FE model BABT sternum impact, where the sternum generally showed lesser BFD due to its stiffness compared to the upper right chest and abdomen. Conversely, for the soft tissues area, the injury thresholds for the deformation-based metrics were greater than their W-IRCs, suggesting that injury may be overpredicted for these regions when using a whole thorax criterion. The kinetic-based metrics had a similar trend to the deformation metrics, except their 50% injury thresholds for the sternum area were all greater.

Overall, grouping impact data into three groups of similar underlying tissues resulted in improved prediction accuracies as measured by ROC AUCs. Additionally, grouping the data highlighted differences between the three location groups when comparing their 50% injury risk thresholds, which generally followed trends expected from the stiffness of the underlying tissues.

4.4 Limitations

The present study had some limitations. Real-world cases include anthropomorphic variability in terms of gross measures (e.g., stature) and local measures (e.g., muscle and adipose tissue thickness). However, the present numerical study used a single human body model that represented a 50^{th} percentile male. Thus, the results from this study corresponded to one male geometry. It is also important to acknowledge that the present study considered eight impact locations, and further studies on smaller variations in location are needed. Loading from the BIBC was applied by way of prescribed displacement at various locations on the thorax. A consistent application of the BABT loading enabled direct comparison of response and injury levels at different thorax locations. However, there may exist a coupling effect between the armor, projectile, and thorax such that the same impact condition could result in differing BFD depending on the underlying tissues. Additional experimental research is required to better understand coupling of the armor and the thorax. It is also crucial to keep in mind that the assessment of prediction accuracy pertains specifically to predicting injuries from the thorax model and further validation of the resulting L-IRCs is required, using a greater number of BABT events. In future studies, it is recommended that anthropomorphic variability be considered along with a wider and finer range of severities and cases that include BABT impact radius and shape.

Finally, the study introduced sBFD as a new criterion to assess BABT injury risk, which may be difficult to measure experimentally in physical tests but could be potentially useful for future simulation methodologies.

5 Conclusions

The present study performed BABT impacts on an advanced human body thorax model and compared the effects of impact location on thoracic responses and injury predictions. Overall, regardless of the consideration of impact location, the IRCs using deformation-based metrics had lesser variability and performed better in predictions than the IRCs using kinetic-based metrics. It was found that sBFD had comparable results in assessing injury risk when compared to BFD for a 50^{th} percentile male. Additionally, it was observed that the impact locations did have a marked effect on injury severity, which led to varying location-specific IRCs. When comparing IRCs calculated for the whole thorax, IRCs calculated for specific locations yielded improved prediction capabilities for the metrics considered. In a future study, a greater variety of impact parameters and anthropomorphic characteristics should be investigated to increase robustness and reduce biases. Overall, this study points the need for consideration of impact location and underlying tissues to improve prediction accuracy of IRCs related to BABT.

6 Acknowledgments

The authors gratefully acknowledge the financial support of the Natural Sciences and Engineering Research Council Discovery Grant Program and the DND NSERC Supplement; a gratefully acknowledge computing resources from the Digital Research Alliance of Canada.

7 Nomenclature

AUC	Area Under the Curve
BABT	Behind Armor Blunt Trauma
BABT-ID	Behind Armor Blunt Trauma Injury Database

BABT-WALT	Behind Armor Blunt Trauma Waterloo Thorax
BFD	Backface Deformation
BIBC	BABT Impact Boundary Condition
CI	Confidence Interval
DND	Department of National Defence
FE	Finite Element
HSTM	Human Surrogate Torso Model
HTFEM	Human Torso Finite Element Model
IRC	Injury Risk Curve
L-IRC	Locational Injury Risk Curve
NSERC	National Sciences and Engineering Research Council
PLC	Pulmonary Lung Contusion
PMHS	Post-Mortem Human Subject
ROC	Receiver-Operating Characteristic
sBFD	Submuscular Backface Deformation
SE	Standard Error
W-IRC	Whole thorax Injury Risk Curve
WSTM	Wayne State Thorax Model
QI	Quality Index

8 References

[1] Prather, R. N., Swann, C. L., Hawkins, C. E., and ARMY ARMAMENT RESEARCH AND DEVELOPMENT COMMAND ABERDEEN PROVING GROUND MD CHEMICAL SYSTEMS LAB, 1977, *Backface Signatures of Soft Body Armors and the Associated Trauma Effects*, Report No. ADA049463, ARMY ARMAMENT RESEARCH AND DEVELOPMENT COMMAND ABERDEEN PROVING GROUND MD CHEMICAL SYSTEMS LAB.

[2] National Institute of Justice, 2008, *Ballistic Resistance of Body Armor*, Standard No. 0101.06, National Institute of Justice.

[3] Carroll, A. W., and Soderstrom, C. A., 1978, "A New Nonpenetrating Ballistic Injury," Ann. Surg., **188**(6), pp. 753–757.

[4] Cronin, D. S., Bustamante, M. C., Barker, J., Singh, D., Rafaels, K. A., and Bir, C., 2021, "Assessment of Thorax Finite Element Model Response for Behind Armor Blunt Trauma Impact Loading Using an Epidemiological Database," J. Biomech. Eng., **143**(3).

[5] Goldfarb, M. A., Ciurej, T. F., Weinstein, M. A., Metker, L. W., and Ground, E. A. A., 1975, *A Method for Soft Body Armor Evaluation: Medical Assessment*, Report No. ADA005575, EDGEWOOD ARSENAL ABERDEEN PROVING GROUND MD.

[6] Wilhelm, M., and Bir, C., 2008, "Injuries to Law Enforcement Officers: The Backface Signature Injury," Forensic Sci. Int., **174**(1), pp. 6–11.

[7] K. A. Rafaels, K. L. Loftis, C. A. Bir, 2018, "Can Clay Tell Us More Than Deformation ?," *Proceedings of the Personal Armour Systems Symposium 2018*, Personal Armour Systems Symposium, p. 8.

[8] Cronin, D. S., 2006, "Detailed Thoracic Model To Investigate Behind Armour Blunt Trauma," *Proceedings of the Personal Armour Systems Symposium*, Personal Armour Systems Symposium, pp. 1–10.

[9] Montanarelli, N., Hawkins, C. E., Goldfarb, M. A., Ciurej, T. F., and ARMY LAND WARFARE LAB ABERDEEN PROVING GROUND, 1973, *Protective Garments for Public Officials*, Report No. ADA089163, ARMY LAND WARFARE LAB ABERDEEN PROVING GROUND MD.

[10] Clare, V. R. Lewis, J. H. Mickiewicz, A. P. Sturdivan, L. M., 1976, *Body Armor: Blunt Trauma Data*, Report No. 32266, National Institute of Law Enforcement and Criminal Justice.

[11] Carr, D. J., Horsfall, I., and Malbon, C., 2016, "Is behind Armour Blunt Trauma a Real Threat to Users of Body Armour? A Systematic Review," J. R. Army Med. Corps, **162**(1), pp. 8–11.

[12] Jennings, R. M., Malbon, C., Brock, F., Harrisson, S., and Carr, D. J., 2018, "A Preliminary Study into Injuries due to Non-Perforating Ballistic Impacts into Soft Body Armour over the Spine," Injury, **49**(7), pp. 1251–1257.

[13] Bir, C., Lance, R., Stojsih-Sherman, S., and Cavanaugh, J., 2017, "Behind Armor Blunt Trauma: Recreation of Field Cases for the Assessment of Backface Signature Testing," 30th International Symposium on Ballistics, **0**(0), pp. 1264–1275.

[14] McMullen, M. J., and Williams, C. J., 2008, "Injuries to Law Enforcement Officers Shot Wearing Personal Body Armor: A 30-Year Review," The Police Chief, **2**(8).

[15] Roberts, J. C., O'Connor, J. V., and Ward, E. E., 2005, "Modeling the Effect of Non-Penetrating Ballistic Impact as a Means of Detecting behind Armor Blunt Trauma," J. Trauma, **58**(6), pp. 1241–1251.

[16] Roberts, J. C., Ward, E. E., Merkle, A. C., and O'Connor, J. V., 2007, "Assessing behind Armor Blunt Trauma in Accordance with the National Institute of Justice Standard for Personal Body Armor Protection Using Finite Element Modeling," J. Trauma, **62**(5), pp. 1127–1133.

[17] Roberts, J. C., Merkle, A. C., Biermann, P. J., Ward, E. E., Carkhuff, B. G., Cain, R. P., and O'Connor, J. V., 2007, "Computational and Experimental Models of the Human Torso for Non-Penetrating Ballistic Impact," J. Biomech., **40**(1), pp. 125–136.

[18] Merkle, A. C., Ward, E. E., O'Connor, J. V., and Roberts, J. C., 2008, "Assessing behind Armor Blunt Trauma (BABT) under NIJ Standard-0101.04 Conditions Using Human Torso Models," J. Trauma, **64**(6), pp. 1555–1561.

[19] Raftenberg, M. N., 2006, "MODELING THORACIC BLUNT TRAUMA: TOWARDS A FINITE-ELEMENT-BASED DESIGN METHODOLOGY FOR BODY ARMOR," *Transformational Science and Technology for the Current and Future Force*, WORLD SCIENTIFIC, pp. 219–226.

[20] Shen, W., Niu, Y., Bykanova, L., Laurence, P., and Link, N., 2010, "Characterizing the Interaction among Bullet, Body Armor, and Human and Surrogate Targets," J. Biomech. Eng., **132**(12), p. 121001.

[21] Cronin, D. S., 2015, "Investigation of Lung Response Resulting from Behind Armour Blunt Trauma Impact Scenarios," *Proceedings of the International Research Council on Biomechanics of Injury*, International Research Council on Biomechanics of Injury.

[22] Metker, L. W., Prather, R. N., and Johnson, E. M., 1975, *A Method for Determining Backface Signatures of Soft Body Armors*, Report No. 34850, EDGEWOOD ARSENAL ABERDEEN PROVING GROUND MD.

[23] Prather, R. N., Metker, L. W., and Ground, E. A. A., 1976, *Ballistic Test Matrix for Kevlar Material*, Report No. ADA029006, EDGEWOOD ARSENAL ABERDEEN PROVING GROUND MD.

[24] Wilhelm, M. R., 2003, "A Biomechanical Assessment of Female Body Armor," Ph.D. dissertation, Wayne State University.

[25] Choudhury, S., Yerramalli, C. S., Guha, A., and Ingle, S., 2022, "Prediction and Mitigation of behind Armor Blunt Trauma in Composite Plate Armor Using Rubber Backing or Air Gaps," European Journal of Mechanics - A/Solids, **93**, p. 104533.

[26] Tilsley, L., Carr, D. J., Lankester, C., and Malbon, C., 2018, "Do Air-Gaps behind Soft Body Armour Affect Protection?," J. R. Army Med. Corps, **164**(1), pp. 15–18.

[27] International Organization for Standardization, 2014, *ISO/TS 18506 Procedure to Construct Injury Risk Curves for the Evaluation of Road User Protection in Crash Tests*, Standard No. 18506:2014, International Organization for Standardization (ISO), Geneva, Switzerland.

[28] Nahm, F. S., 2022, "Receiver Operating Characteristic Curve: Overview and Practical Use for Clinicians," Korean J. Anesthesiol., **75**(1), pp. 25–36.